Macromolecules

Article

pubs.acs.org/Macromolecules

Prefracture Instabilities Govern Generation of Self-Affine Surfaces in Tearing of Soft Viscoelastic Elastomeric Sheets

Sandip Patil, Amit Ranjan,† and Ashutosh Sharma*

Department of Chemical Engineering and DST Unit on Nanosciences, Indian Institute of Technology, Kanpur, India

Supporting Information

ABSTRACT: We present an experimental study on fracture behavior of soft viscoelastic network solid films of polydimethylsiloxane (PDMS) and morphology of the fracture-generated surfaces. The most interesting behavior is the generation of fractal patterns when the storage and loss moduli are comparable. We find the formation of isolated defects and cracks ahead of the fracture-front. The observed morphology of the torn surfaces is correlated to the prefracture behavior by studying the crack propagation and coalescence. Tearing of PDMS containing 2% cross-linking agent with a terminal elastic modulus, G', of 10 kPa, shows distinct crack patterns at different tearing speeds. Slower tearing leads to the formation of dendritic patterns of propagating fingers, whereas at the higher deformation-rates, more frequent nucleation of bubble like defects occurs. The propagating fingers develop undulations along its sides. The effects of tearing speed on the length scale of the undulations and the bubbles are studied. The formation of undulations can be explained as a result of Saffman−Taylor instability with a modified *effective* surface tension which accounts for the dissipative energy loss. We also study the rate of formation of the defects, which is shown to be an activated process in that they form beyond a threshold value of the local stress.

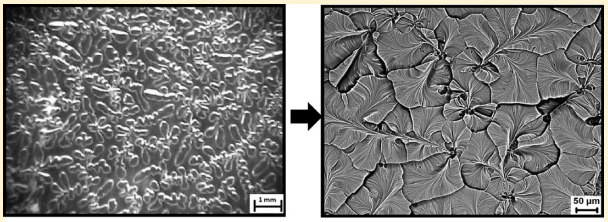

INTRODUCTION

Materials undergo cohesive failure by crack formation and propagation under excessive stress. Study of precrack events and morphology of cracks provides vital clues regarding the nature of the texture generated on the surfaces formed by the fracture and can also be a diagnostic tool for characterizing the failure mechanisms and the properties of the failed material. Materials with different mechanical properties exhibit different morphologies on their fractured surfaces. Ductile fracture in metals[1−3] is accompanied by plastic deformation prior to the fracture where the microvoids coalesce leading to a dimpled, irregular, and rough morphology commonly known as the cup-and-cone morphology. Brittle fracture in metals involves cleavage along crystallographic planes resulting into relatively smoother or faceted surfaces.[4,5] Fracture in polymeric materials has particularly drawn considerable scientific interest because of the complexity of the phenomena and richness of the resulting morphologies. In elastomers such as vulcanized polybutadiene,[6−8] vertical steps separating smooth regions form the characteristic features, whereas in the glassy polymers such as polystyrene, poly(methyl methacrylate), and polycarbonate, periodic micro/nano structured gratings are formed on the fractured surfaces.[9] Spatiotemporal patterns have been observed in peeling of adhesive tapes.[10] While adhesive interfacial failure of elastomeric surfaces have been extensively studied,[11−14] patterns formed by tearing of elastomeric sheets have not been explored. Previous studies on interfacial debonding have shown both bulk and interfacial fingering instabilities and cavitation during separation.[11,12,15,16] Interfacial debonding of both elastic[13] and viscoelastic adhesive layers[13,14] generate intricate surface structures including fractally rough surfaces during peeling.[14] Analysis of rough surfaces formed in fractured hydrogels has revealed interesting physics.[17,18] Surface instabilities without fracture, such as wrinkling by release of stresses, have also been studied.[19,20]

Here we explore the process and morphology of cohesive fracture in tearing of soft thin viscoelastic polydimethylsiloxane (PDMS) layers and the morphology of the torn surfaces thus generated. In particular, we focus on the chain of events starting from the generation of defects in the prefracture phase, their modifications during the crack propagation and the roles of these processes in determining the eventual surface morphology of completely torn surfaces. In order to assess the role of viscoelasticity, the fracture events and the resulting surface morphologies are studied at different tearing velocity. The morphology of the torn surfaces show novel patterns possessing different features at different length scales which also depend upon the tearing rate. The viscoelastic nature of the material strongly influences the generation and propagation of cracks which ultimately coalesce to cause fracture and form a particular surface morphology. Further, we show that the most interesting patterns in the form of self-affine fractal surfaces are observed only in a narrow range of elastic modulus ($G' \sim 1$ KPa to 10 KPa) of the elastomer. The structure of this paper is as follows: First, we

Received: October 19, 2011
Revised: December 28, 2011
Published: February 6, 2012

describe the details of the experimental setup, methodology, and the materials used. Subsequently our results are presented in two parts. In the first part, we discuss the morphology of the fracture generated surfaces resulting from the cohesive fracture of the elastomeric thin films. In the second part, we analyze the crack formation and propagation in the films while they are being fractured. On the basis of the crack behavior observed before the fracture and the final morphology of the fractured surface, we finally propose a simple physical model correlating the two.

MATERIALS AND METHODS

Sylgard-184 (a two part thermoset silicone elastomer; Dow Chemicals, USA) consisting of oligomer and cross-linking agent was used to prepare Polydimethylsiloxane (PDMS) in this study. The elastomer and cross-linking agent were mixed in the ratio of 100:2 by weight in order to make 2% cross-linked elastomer.[21,22] The solution was prepared in a 25 mL clean glass beaker and degassed under vacuum in order to remove trapped air from the solution. The prepared solutions were cast between two clean glass plates (Figure 1a) with predetermined gap controlled by inserting spacers of known heights between the plates. After casting, prepared solutions were cured at 85 °C for 48 h giving PDMS films of desired thickness. The elastic modulus, G' and loss modulus, G'' for the 2% cross-linked PDMS samples were separately measured at various temperatures by the oscillatory parallel plate method (Anton Paar MCR-501) as functions of frequency. Time−temperature superposition was used to construct the plot for the rheological response (Figure 5a).

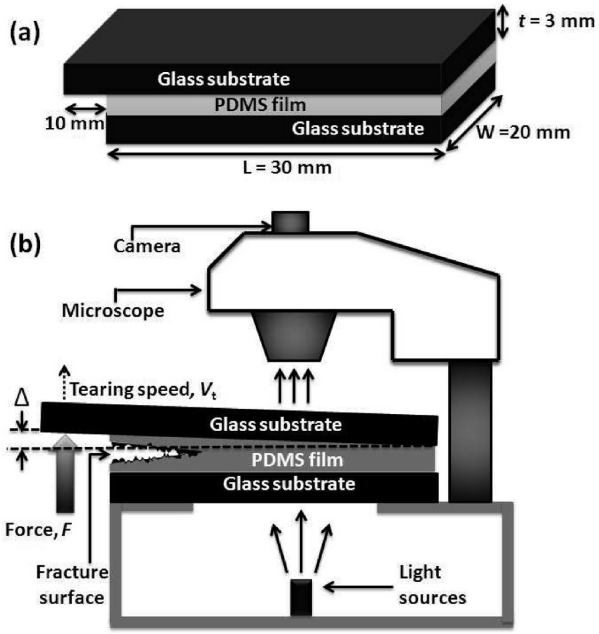

Figure 1. (a) PDMS film cast and bonded between the two glass plates. Typical dimensions of the glass plates are shown. (b) Experimental setup for tearing of PDMS film. The bottom glass plate is strongly attached to a rigid platform and the top plate is lifted from its hanging edge. Force F is applied by a micromanipulator causing a vertical displacement Δ and cohesive fracture in the film.

Figure 1b shows the tearing process in which the film sandwiched between the glass substrates was torn by lifting the hanging edge of one of the glass plates by a micromanipulator with controlled tearing speed, V_t, by applying a force, F on the edge. Application of F causes the point of application to move vertically by a distance Δ. The applied force was recorded using a load cell interfaced with a computer through a data acquisition card. During separation, the adhesive force between the film and glass substrate is much stronger than the cohesive force in the film, thus allowing cohesive fracture during separation. As shown in Figure 2, the most interesting cellular fractal morphologies were found only in the PDMS layers with the cross-linker concentration close to 2% (w/w), which produced a soft elastomeric solid of comparable storage and loss moduli at the time scales (frequencies) involved in the fracture. The rheology of these layers marks the border between transition from the liquid-like to solid-like behavior.[23,24] At relatively low cross-linker concentration of 0.5−1.5%, cracks propagated as the smooth Rayleigh fingers characteristic of cohesion failure in liquids. Beyond 2.5% cross-linker, fracture of elastic layers produced only disjointed craters on the surface.

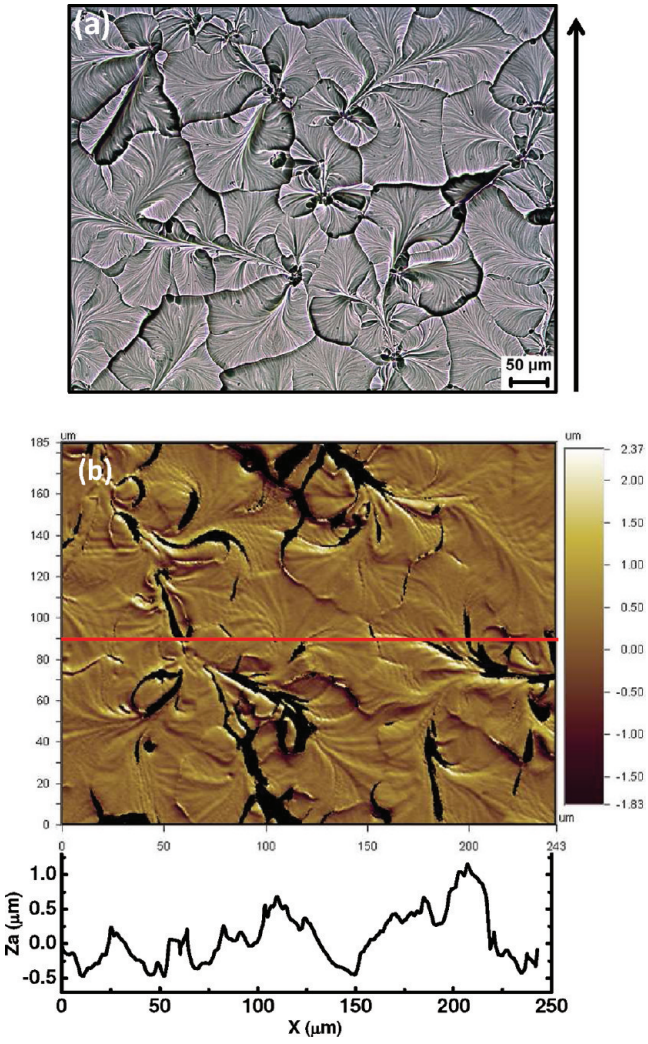

Figure 2. (a) Typical optical micrograph of the torn surface of a soft viscoelastic PDMS layer. The right side arrow signifies the direction of tearing. (b) Optical profilometry micrograph showing surface topography of the torn film of thickness $h \approx 20$ μm (roughly half of the total thickness) and tearing speed =100 μm/s.

RESULTS AND DISCUSSION

Morphology of Fracture-Generated Surfaces in Viscoelastic PDMS Layers. We first present the surface morphology of cohesive-fractured or torn viscoelastic PDMS films. The fracture was induced by tearing of homogeneous PDMS films bonded with two confining glass substrates. Fractured surfaces show novel fractal morphologies with cellular micropatterns on the torn surface of PDMS in which

dx.doi.org/10.1021/ma202339y | Macromolecules 2012, 45, 2066−2073

the ridged domains are separated as cells. One such typical morphology of torn surface is shown Figure 2a. The overall appearance of the domains on this scale is akin to leaves or petals. The surface profile was analyzed by surface topography analysis using optical profilometry (Wyko NT-1100) (a cross-section is shown in Figure 2b). The area of examination under microscope was 182 × 142 μm^2. The topographical surface characteristics such as the root-mean-square (RMS) roughness as well as fractal dimension were obtained to characterize these surfaces at different tearing rates. The surface roughness defined by the following relation was found to be 0.5 μm at a tearing speed of 100 μm/s:

$$R_q = \sqrt{\frac{1}{N}\sum_{i=0}^{N}(Z_i - Z_a)^2} \quad (1)$$

Here, Z_a is the average of the Z (height) values within the given area Z_i is the Z value at a given point, and N is the number of sampled points within the given area.

Figure 3 also shows a typical power spectral density curve of the fractured surface which gives the fractal dimension of the surface by the following relation:[25]

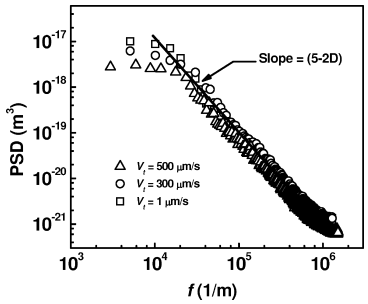

Figure 3. Power spectral density curves for V_t = 1, 300, and 500 μm/s for thickness h = 20 μm (half of the total thickness). The slope gives a value for the fractal dimension of the morphology close to 1.5.

$$S(f) = \frac{c}{f^{(5-2D)}} \quad (2)$$

Here f is the wavenumber, $S(f)$ is the power spectral density, C is a scaling constant, and D is the fractal dimension. The low f limit corresponds to the sample-size and the high f limit corresponds to the Nyquist frequency corresponding to the resolution limit of the analysis. The fractal dimension, D, can be obtained by extracting the slope of the power spectral density (PSD) function on a log−log plot as suggested by eq 2. The fractal dimension of the surface was found close to 1.5 independent of the tearing speed in the range of 1−500 μm/s. This value of the fractal dimension signifies that the height variation follows a Wiener process.[26,27] Interestingly, although the tearing speed altered the characteristic length scales of the pattern, it did not change its characteristic fractal dimension. The effect of layer thickness was more interesting. Increase in thickness increased the petal-leaf size without changing the overall apearance of the pattern as shown in Figure 4.

Prefracture Events in Soft Viscoelastic Elastomers. Fracture in viscoelastic elastomers is a complex and poorly understood phenomenon. According to the current understanding,[28,29] a processing zone lies in the immediate proximity to a blunted crack tip where energy is primarily dissipated through plastic deformation, chain-breakage and flow. An elastic zone lies further away from the crack tip where the energy is stored in an elastically strained material. Owing to the viscoelastic nature of the elastomer used, the behavior of crack propagation can be influenced by the crack speed. There are several theoretical and experimental studies on the instabilities in adhesive or interfacial failure seen in the peel experiments,[13,30−34] but a petal-leaf morphology shown here in the cohesive rupture has not been reported.

In what follows, we present the development of precrack morphologies within the still intact layer away from the crack line that tears the layer in two. The results are discussed for the 2% cross-linker containing PDMS films, which invariably yielded fractal morphologies upon completion of fracture. In order to gain an understanding of the processes involved in morphological development, rheological characterization of the

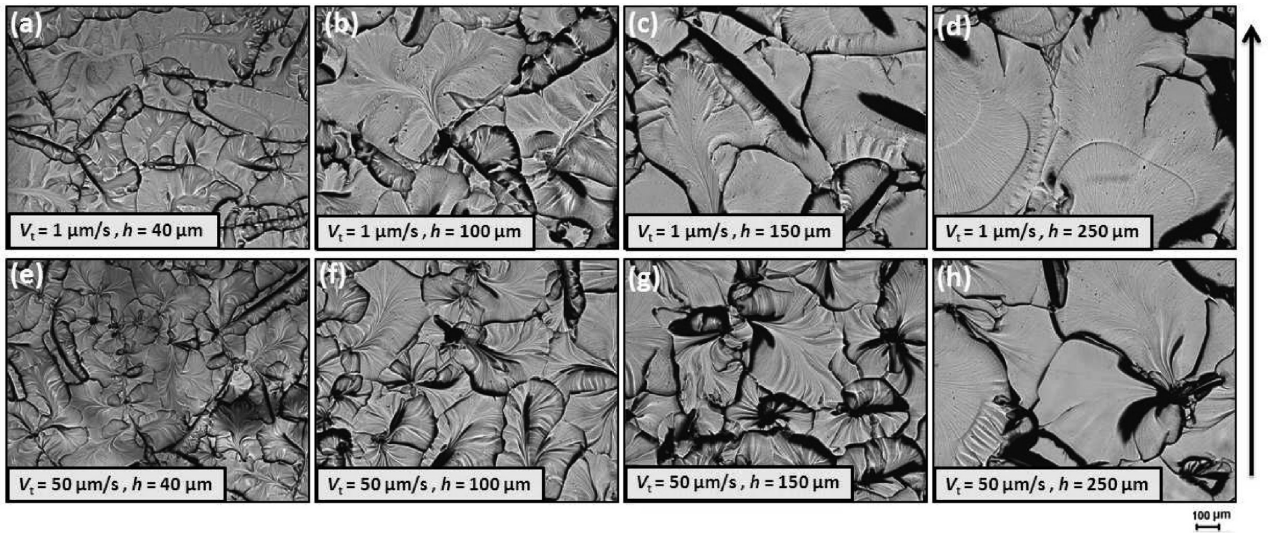

Figure 4. Optical micrographs of fractured surfaces of 2% cross-linked PDMS films with different thickness and tearing speed. Right side arrow indicates tearing direction of the film.

dx.doi.org/10.1021/ma202339y | Macromolecules 2012, 45, 2066−2073

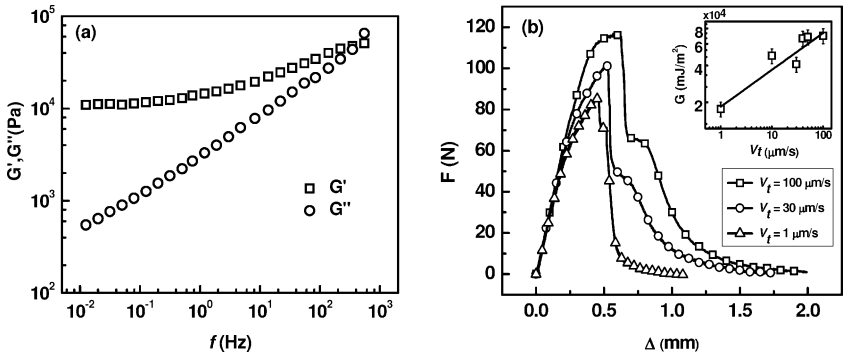

Figure 5. (a) Oscillatory response of 2% PDMS showing storage (squares) and loss (circles) modulus obtained using time−temperature superposition. (b) Force-displacement curves generated while tearing at three different tearing velocities. Inset shows the energy as a function of tearing speed curve for 40 μm thickness following a power law behavior with an exponent of 1/3.

PDMS networks was first performed. The oscillatory response of a 2% cross-linked PDMS sample obtained by time−temperature superposition is shown in Figure 5a. Rheology data confirms that the material is a soft viscoelastic solid made of an imperfect network.[34] In our study, the vertical tearing speed, V_t, of the plate lift-off ranged from 1 to 100 μm/s, which resulted in about 2 orders of magnitude variation also in the crack propagation speed, $V_c \sim 100\ V_t$ ($V_c \sim 100$−10000 μm/s).

For a film with the thickness h = 40 μm, the range of crack propagation speed corresponds to the frequency f (or the deformation rate, $f = V_c/h$) ranging from around 2 to 300 Hz. This range of frequency relevant to our experiments is close to the "transition region" in the frequency sweep rheological measurement of 2% cross-linked PDMS films. A characteristic of this regime is that both storage and loss moduli are comparable and increase with frequency. Therefore, both storage and dissipation of energy are about equally important in our experiments, although the terminal behavior of the material is that of a solid.

We first present the force vs. separation behavior for 2% cross-link films of 40 μm thickness. The force-separation curves at three different speed of tearing are shown in Figure 5b. The shapes of these curves are typical of pressure-sensitive adhesives. The initial linear rise in the force is caused by the stored elastic energy. The film starts to rupture beyond a critical stress and the energy is now released leading to a drop in the stress. The work done is now distributed between the dissipative loss and the energy of formation of new surfaces as the precrack structures form, reorganize as cracks and propagate in the material leading to fracture. The storage and loss are strongly dependent on crack propagation velocity which determines the effective shear rate of the system given by $f = V_c/h$, where f is the frequency, V_c is the crack propagation velocity, and h is the thickness of the film. The energy released can be calculated from the area under the force−distance curve beyond the critical stress where the force undergoes a sharp drop due to crack initiation. A plot of energy released per unit area as a function of fracture speed in the inset of Figure 5b shows a power law dependence with an exponent of 1/3. This exponent has been predicted by Persson and Brener.[28] Their model, essentially applicable to relatively high velocities such that the material lies in the 'transition regime' of frequency, accounts for the dissipative losses occurring near the crack tip. From the rheological data in Figure 5a, the onset of transition regime in our samples is expected for f > 10 Hz, and hence for crack propagation velocities larger than 400 μm/s. Since crack-propagation velocity ranges from 100 μm/s to 10000 μm/s, samples in most of our cases lie in the "transition regime" of rheological behavior. Thus, the data presented in Figure 5b confirms the prediction of Persson and Brener and underlines the importance of dissipative loss in the energetics of the tearing process.

We now examine the dynamics and morphology of the precrack patterns that form in the still intact layer beyond the propagating fracture front. As the upper plate was lifted, accumulated elastic stresses begun to relax by the formation of bubbles/cavities and fingers as shown in Figure 6. These formations are important for the understanding of the observed postfracture cellular micropatterns. The length scale and morphology of these precrack patterns shows dependence on the speed of tearing. Snapshots of the crack patterns in the layers fractured at different tearing speeds are presented in Figure 6. At low tearing speeds, (Figure 6a−c) long fingers or crack lines which develop side undulations dominate the pattern, whereas at high tearing speeds (Figure 6d−f) both bubbles as well as shorter and less well-defined crack-lines appear. These features lead to a pattern dominated by the long dendritic lines at low velocity, and a more uniform cellular pattern at high tearing velocities. In the case of low tearing velocity, the fine stems of the postfracture leaf pattern shown in Figure 2 correspond to the crack lines witnessed in Figure 6c. Nucleation of isolated bubbles or cavities is not witnessed at low tearing speeds, indicating more viscous behavior. The less defined crack-lines or fingers and a greater proportion of elongated bubbles are characteristic of more elastic behavior at higher tearing speeds. Indeed, propensity for the formation of fingers without bubbles in a viscoelastic liquid layer of 0.5% cross-linked PDMS corresponding to a viscous dominated behavior is clearly seen in Figure 6g. However, an elastic 4% cross-linked layer only forms bubbles instead of fingers as shown in Figure 6h. The side branches or waviness of the crack lines or fingers in Figure 6a, b, c were found to disappear on removal of tearing stress or by reversing the direction of tearing arm leading to crack closing (see Supporting Material). However, the main crack-lines were irreversible and remained after the removal of stress. This confirms that the side undulations originate from liquid-like Saffman−Taylor fingering instabilities. However, the long fine crack lines and the bubbles/cavities once formed persisted even after the removal of stress. Therefore, the fully formed crack lines/bubbles are characteristic of solid-like rupture caused by chain breakage and irreversible plastic deformations. These images suggest two length scales of interest: (i) λ_f, the length

dx.doi.org/10.1021/ma202339y | Macromolecules 2012, 45, 2066−2073

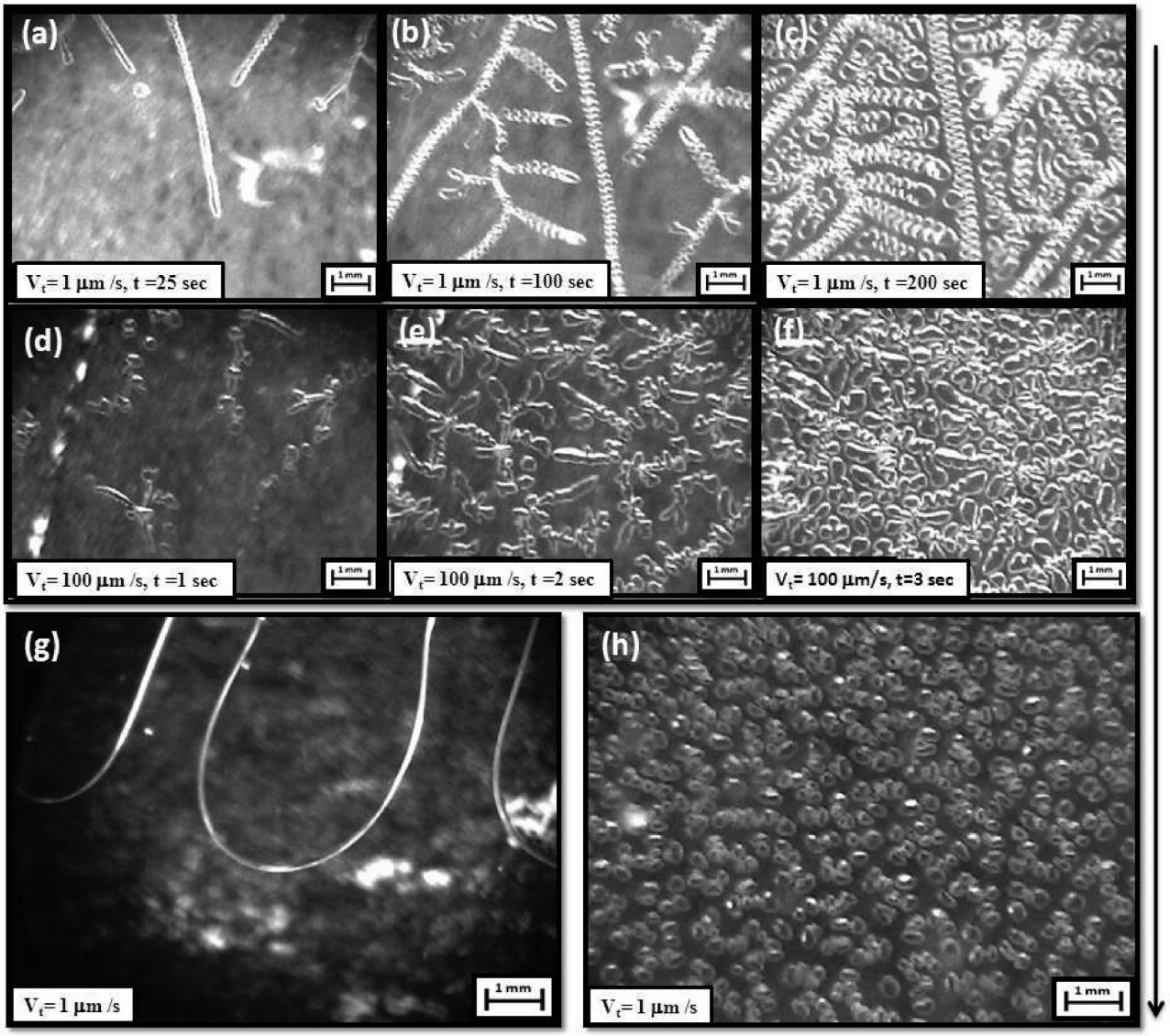

Figure 6. (a) Real time optical micrographs of precracks in 2% cross-linked 40 μm thick PDMS layers at different tearing speeds. First (a, b, c) and second (d, e, f) rows correspond respectively to V_t = 1 and 100 μm/s. Snapshots at three different times are presented for each tearing speed. (g, h) Real time optical micrographs of 0.5% and 4% cross-linker containing PDMS layers at tearing speed of V_t = 1 μm/s. Arrow on the right side of the figure shows direction of the crack propagation.

scale of the undulations appearing along the lateral boundaries of the linear fingers, and (ii) λ_b, the average distance between two crack-features (bubble or fingers). The former length scale is independent of time and as mentioned before, is found to depend on the liquid-like nature of the films. The latter which originates from the solid-like behavior of the film, depends on density of nucleated cracks and is therefore time dependent. We first address λ_f which shows a very weak but systematic variation with speed. We propose that the undulations in the finger like structures is due to a Saffman−Taylor like instability that arises along the interface of two liquids when a less viscous liquid is driven against a more viscous one in Hele−Shaw kind of geometry.[35] This effect has already been studied in adhesive failures occurring in viscoelastic materials using probe-tack experiments.[23] However, our studies gain a further understanding into the phenomena and establish the importance of viscous dissipation prevalent in the crack processing zone. We show that the dissipative energy loss plays an important role in determining the length scales of these modulations.

Variation of λ_f with V_t, the tearing speed, is presented in Figure 7 It is observed to systematically increase with speed and have a weak power-law dependence. This weak variation can be explained by combining the idea of Saffman−Taylor instability in liquid interfaces and Persson and Brener's result.[28] Saffman−Taylor instability arising in the interface between two liquids of unequal viscosity when the one with lower viscosity is driven against the other, results into surface undulations with a characteristic wavelength given by the following formula:[23]

$$\lambda_f \approx \frac{\pi h \sqrt{\gamma}}{\sqrt{\eta V_c}} \tag{3}$$

where λ_f is the wavelength of the instability appearing along the sides of the fingers, h is the film thickness, γ is the surface energy per unit area, and η is the viscosity of the medium.

dx.doi.org/10.1021/ma202339y | Macromolecules 2012, 45, 2066−2073

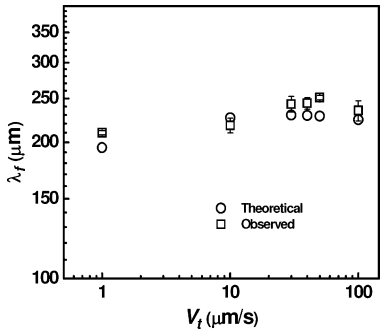

Figure 7. Wavelength variation with tearing speed with a constant thickness (h = 40 μm). Squares represent the experimentally observed values, and circles represent the theoretically calculated values that account for interfacial instability and viscous dissipation.

The viscosity, η can be estimated from the oscillatory rheology data by $\eta = ((G'^2) + (G''^2))^{1/2}/f$ where G' is the storage modulus and G'' is the loss modulus. Nase et al.[23] studied the finger formation in PDMS networks at different velocities using probe-tack test and found that λ_f decreases with velocity. These authors were able to fit their feature wavelengths to the above expression applicable to interfacial instability caused by the Saffman−Taylor like mechanism. However, in our case, we observe a systematic increase in λ_f with velocity although the dependence is very weak. Our data suggests, as argued in the next paragraph, that the origin of this weak dependence lies in the dissipative dynamics operating in the crack's vicinity. Persson and Brener calculated γ_{eff}, an effective surface energy per unit area by accounting for the dissipation in the surrounding region of the propagating cracks, and defining the γ_{eff} as follows:

$$\gamma_{eff} = 2G \tag{4}$$

Here G is the energy released per unit area at any given V_c, the crack tip velocity, and is given by the following expression:

$$G = G_o(1 + f(V_c)) \tag{5}$$

Here G_o is the energy released in the static limit, and $f(V_c)$ is the correction due to velocity dependent dissipation. Their result for γ_{eff} as a function of crack tip velocity is summarized by the following relation:

$$\gamma_{eff} = \gamma_o\left(\frac{V_c}{V_o}\right)^{1/3} \tag{6}$$

Equation 6 was obtained for the Rouse like relaxation of the chains which predicts that G'' scales as $f^{1/2}$. As seen in the rheological response in Figure 5a, our samples also show a scaling exponent close to 0.5, which justifies the use of eq 6. Where γ_o is the surface tension of the material in the low velocity limit, and $V_o \approx a_o/\tau$ where a_o is the size of the core region having a value close to atomic dimension and τ is the relaxation time of the network, which in our case is around 0.003 s (Figure 5a). Substituting γ_{eff} for γ, the surface energy, in Saffman−Taylor expression of eq 3, we obtain a final expression for a wavelength resulting from a Saffman−Taylor instability that also accounts for the dissipative losses. The experimental data and the theoretically predicted dependency of the wavelength on velocity are presented in Figure 7 and show an excellent agreement. Therefore, we argue that this weak dependence can originate from the dissipative dynamics and flow predominantly occurring in the immediate vicinity of the fingers.

Next we turn our attention to the phenomena of nucleation of cracks at different tearing speeds. At higher tearing speeds, formation of new voids that elongate into finger like patterns and branching of pre-existing fingers become more frequent. In quantification of defect density, every disjointed feature such as voids and the side-branch features were counted as defects. Our data show, as we argue next, that nucleation of these defects is an activated process. To this end we calculate dN/dt, the number of such defects formed per unit time, for the 40 μm thick film in a reference area at a distance of 10 mm from the edge of the film and 20 mm from the point of application of tearing force. dN/dt is measured by counting the number of defects, $N(t)$ in the reference area. For an activated process, the rate of nucleation is given by $dN/dt \propto e^{(-E_b/kT)}$ where E_b is the energy barrier.[36] We propose that the local elastic energy in a reference volume V, has to surmount a threshold energy ε, to activate the nucleation process. Here V and ε are unknown constants. If σ is the local stress, and μ is the bulk modulus, then local elastic energy in the reference volume is given by σ^2V/μ, such that the local energy barrier is $E_b = \varepsilon - (\sigma^2V/\mu)$. Therefore, the rate of nucleation is given by the following equation:

$$\frac{dN}{dt} \propto e^{[(1/kT)\{(\sigma^2V/\mu)-\varepsilon\}]} \tag{7}$$

Therefore, at constant temperature, the rate of nucleation at any point in the sample is proportional to $e^{((\sigma^2V)/(kT\mu))}$. For a crack propagating at a speed V_c, the local stress at a point located at a distance x_o from the edge of the plate at any time t is given by the following function:[1]

$$\sigma \approx \frac{K}{\sqrt{x_o - V_c t}} \tag{8}$$

where K is the stress intensity factor. The term under square-root in the denominator is the distance of the concerned point from the crack edge. A combination of eqs 7 and 8 predicts that logarithm of dN/dt should vary linearly with $1/(x_o - V_c t)$, which we indeed observe as shown in Figure 8. Thus, our results suggest

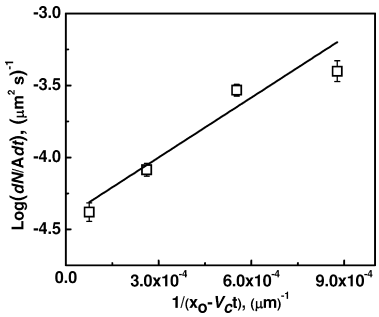

Figure 8. Dependency of the logarithm of nucleation rate per unit area with $1/(x_O - V_C t)$.The linear best fit line suggests that generation of the cracks is an activated process.

that the formation of cracks is an activated process where the activation energy keeps decreasing as the stress level increases with time, thereby leading to more frequent formation of cracks.

Another interesting observation in our experiments is that the fingers that otherwise keep elongating with time, tend to

dx.doi.org/10.1021/ma202339y | Macromolecules 2012, 45, 2066−2073

stop as soon as they are met at their tip with another pre-existing finger, that is, the fingers avoid intersecting each other. Majumder et al.[37] have also observed that propagating fingers formed as a result of peeling an adhesive slows down as they meet a microchannel running perpendicular to their direction of propagation. This phenomena can be explained by noting that as the tip of a finger of a later generation (secondary) approaches a pre-existing finger (primary) from sideways, the region lying ahead of the tip of the secondary finger where the elastic energy of the secondary finger gets released, can be assumed to be a composite of PDMS medium and air present inside the primary finger.

Thus, the effective modulus of this region is significantly reduced because of the presence of a pre-existing air-filled void. This effective modulus keeps becoming smaller as the secondary tip approaches the primary finger since the volume fraction of the neighboring region of the tip is increasingly dominated by air. As a result, the propagation of the secondary fingers is impeded because their further advancement does not lead to a significant release in stored elastic energy at the expense of exposing new surface. Another explanation of this observation could be that once finger-boundaries come very close, the stress is concentrated in the region between the fingers which leads to elongation of the material along the applied stress direction leading to fibril like formation, and consequently, further propagation of the fingers is not observed.

After the dynamic behavior of the propagating cracks, we next describe the correlation between the observed features in fracture generated surfaces and the coalesced crack pattern immediately before fracture. At larger separation speeds, the resulting surfaces invariably form cellular areas patterned with ridge-like formations. The cellular domains appearing in the postfracture images essentially are those surfaces which get exposed at the time of formation of the nascent cracks/bubbles.

Spans of these cellular domains correspond to the defects that coalesce immediately before fracture. The distance between the coalesced cells in the crack pattern observed right before fracture compares favorably with the typical size of the cells observed in the fracture generated surfaces. The points of rupture define the boundary of these cellular domains as well as the vertical protrusions in the surface of the films predominantly responsible for the rms roughness measured in the profilometry experiments. A schematic model correlating prefracture processes and the observed crack patterns as well as the finally observed surface morphology in the fractured surface is shown in Figure 9.

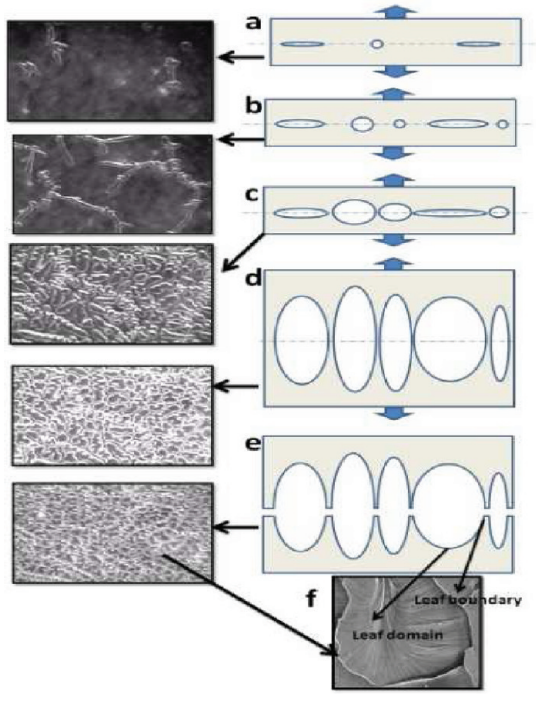

Figure 9. Proposed schematic model correlating prefracture processes, observed crack patterns, and the final surface morphology.

CONCLUSIONS

In summary, we have studied the tearing velocity dependence of crack formation in those soft viscoelastic films which form self-affine cellular micropatterns on fracture, and showed that during fracture, the nucleation of cracks is affected by the solid-like properties of the films. Fingers or bubbles nucleate after a sufficient accumulation of local stress. Exceeding the critical stress causes random breaking of the bonds resulting into rupture and thereby nucleation of cracks. During the course of fracture, the liquid-like instability in the medium generates undulations along the sides of the propagating cracks. In particular, two phenomena of (i) Saffman−Taylor instability of the interface and (ii) the dissipative loss in the vicinity of the propagating cracks govern the length scale of these undulations. Finally a correlation of the observed surface structure to the crack pattern formed right before fracture is established.

ASSOCIATED CONTENT

Supporting Information

Crack opening and closing videos. This material is available free of charge via the Internet at http://pubs.acs.org/.

AUTHOR INFORMATION

Corresponding Author

*E-mail: ashutos@iitk.ac.in. Telephone: +91-512-2597026. Fax: +91-512-2590104.

Present Address

[†]Department of Chemical Engineering, Rajiv Gandhi Institute of Petroleum Technology, Raebareli, India

ACKNOWLEDGMENTS

This work was supported by the DST, New Delhi, by its Unit on Soft Nanfabrication and by an IRHPA grant.

REFERENCES

(1) Dieter, G. E. *Mechanical Metallurgy*; McGraw-Hill: London, 1988.
(2) Wilsdrof, H. G. F. *Mater. Sci. Eng.* **1983**, *59*, 1−39.
(3) Thomason, P. F. *Acta. Mater.* **1999**, *47*, 3633−3646.
(4) Pugh, S. F. *Br. J. Appl. Phys.* **1967**, *18*, 129−162.
(5) Ravi-Chandar, K.; Yang, B. *J. Mech. Phys. Solids.* **1997**, *45*, 535−563.
(6) Gent, A. N.; Pulford, C. T. R. *J. Mater. Sci.* **1984**, *19*, 3612−3619.
(7) Cam, J.-B.; Le; Toussaint, E. *Macromolecules* **2010**, *43*, 4708−4714.
(8) Mathew, A. *Eur. Polym. J.* **2001**, *37*, 1921−1934.
(9) Pease, L. F.; Deshpande, P.; Wang, Y.; Russel, W. B.; Chou, S. Y. *Nat. Nanotechnol.* **2007**, *2*, 545−548.
(10) Yamazaki, Y.; Toda, A. *J. Phys. Soc. Jpn.* **2004**, *73*, 2342−2346.
(11) Crosby, A. J.; Shull, K. R.; Lakrout, H.; Creton, C. *J. Appl. Phys.* **2000**, *88*, 2956−2966.
(12) Shull, K.; Flanigan, C.; Crosby, A. *Phys. Rev. Lett.* **2000**, *84*, 3057−3060.
(13) Ghatak, A.; Chaudhury, M. K. *Langmuir* **2003**, *19*, 2621−2631.
(14) Persson, B. N. J.; Kovalev, A.; Wasem, M.; Gnecco, E.; Gorb, S. N. *Europhys. Lett.* **2010**, *92*, 46001−p4.

(15) Yamaguchi, T.; Koike, K.; Doi, M. *Europhys. Lett.* **2007**, *77*, 64002−p5.
(16) Nase, J.; Creton, C.; Ramos, O.; Sonnenberg, L.; Yamaguchi, T.; Lindner, A. *Soft Matter* **2010**, *6*, 2685−2691.
(17) Tanaka, Y.; Fukao, K.; Miyamoto, Y. *Eur. J. Phys. E* **2000**, *401*, 395−401.
(18) Baumberger, T.; Caroli, C.; Martina, D.; Ronsin, O. *Phys. Rev. Lett.* **2008**, *100*, 178303−4.
(19) Yang, S.; Khare, K.; Lin, P.-C. *Adv. Funct. Mater.* **2010**, *20*, 2550−2564.
(20) Lin, P.-C.; Yang, S. *Soft Matter* **2009**, *5*, 1011−1018.
(21) Mukherjee, R.; Pangule, R. C.; Sharma, A.; Banerjee, I. *J. Chem. Phys.* **2007**, *127*, 064703−6.
(22) Gonuguntla, M.; Sharma, A.; Mukherjee, R.; Subramanian, S. A. *Langmuir* **2006**, *22*, 7066−7071.
(23) Nase, J.; Lindner, A.; Creton, C. *Phys. Rev. Lett.* **2008**, *101*, 074503−4.
(24) Arun, N.; Sharma, A.; Pattader, P.; Banerjee, I.; Dixit, H.; Narayan, K. *Physi. Rev. Lett.* **2009**, *102*, 254502−4.
(25) Berry, M. V.; Lewis, Z. V. *Proc. R. Soc. London A* **1980**, *370*, 459−484.
(26) Majumdar, A.; Bhushan, B. *J. Tribol.* **1990**, *112*, 205−216.
(27) Barabási, A.-L.; Vicsek, T. *Phys. Rev. A.* **1991**, *44*, 2730−2733.
(28) Persson, B.; Brener, E. *Phys. Rev. E.* **2005**, *71*, 036123−8.
(29) Derks, D.; Lindner, A.; Creton, C.; Bonn, D. *J. Appl. Phys.* **2003**, *93*, 1557−1566.
(30) Ghatak, A.; Chaudhury, M. K.; Shenoy, V.; Sharma, A. *Phys. Rev. Lett.* **2000**, *85*, 4329−4332.
(31) Creton, C.; Leibler, L. *J. Polym. Sci., Polym. Phys.* **1996**, *34*, 545−554.
(32) Ghatak, A.; Mahadevan, L.; Chung, J. Y.; Chaudhury, M. K.; Shenoy, V. *Proc. R. Soc. London A* **2004**, *460*, 2725−2735.
(33) Ghatak, A.; Mahadevan, L.; Chaudhury, M. K. *Langmuir* **2005**, *21*, 1277−1281.
(34) Rubinstein, M.; Colby, R. H. *Polymer Physics*; Oxford University Press: London, 2003.
(35) Saffman, P. G.; Taylor, G. *Proc. R. Soc. London A* **1958**, *245*, 312−329.
(36) Krausz, A. S.; Krausz, K. *Fracture Kinetics of Crack Growth*: Kluwer Academic publisher: Dordrecht, The Netherlands, 1988.
(37) Majumder, A.; Ghatak, A.; Sharma, A. *Science* **2007**, *318*, 258−261.